

Path Planning and Force Control of a 4WD4WS Vehicle

Penglei Dai and Jay Katupitiya

University of New South Wales, Australia

p.dai@student.unsw.edu.au, j.katupitiya@unsw.edu.au

Abstract

The aim of this paper is to develop a system where forces at the wheels of a ground vehicle are controlled to guide the vehicle along a predetermined path. The 7-order Bézier curves are applied to path planning and path tracking, and provide profiles of velocities and accelerations for the mass centre of a 4WD4WS vehicle. The vehicle is considered to be a rigid body with known inertia and mass. The dynamic model used for force control is developed for the determination of the reference forces and steering angles at four independent wheels. The slip angles are also considered in the dynamic model built. The desired forces and steering angles obtained are then used to control the drive forces and the steering angles at individual wheels to guide the vehicle along the planned path. Simulation results are provided to validate the proposed methodology.

Keywords: Force control, ground vehicles, modelling, Bézier curve, path planning.

1 Introduction

One of the key complexities associated with the guidance of large scale ground vehicles that operate in semi- or unstructured environments is the significant amount of lateral and longitudinal slip present. Most methodologies developed for non-holonomic vehicles are not acceptable due to the non-holonomic constraint not being satisfied. The demand for high accuracy navigation at high speeds is ever increasing, especially in agriculture and highway maintenance such as lane marking. Developing error models or offset models to achieve accurate path tracking does not deliver the expected performance due to poor quality of the kinematic or dynamic models used. Despite the considerable efforts put towards the design of controllers using such models, the final

achievements in terms of the controller performance are less than satisfactory. This work presents a platform and a methodology to achieve a more robust solution.

There is an abundance of literatures that present kinematic modelling of ground vehicles [Yalcin *et al.*, 2006] [Tham *et al.*, 1999] [Maalouf *et al.*, 2006], in which the control inputs are velocities and the vehicles are subjected to low accelerations (to minimize the inertial effects) and low speeds (to minimize the radial accelerations during cornering). The majority of the kinematic models deal with non-holonomic systems - the systems that are not subjected to lateral slip. In terms of dynamics, some researchers have proposed traction control of robotic vehicles by the optimization of power consumption or ground contact forces [Iagnemma and Dubowsky, 2004] [Waldron and Abdallah, 2007]. However, the skid steering mechanism of vehicles in these studies restrict the mobility and flexibility of vehicles, especially in occasions where high speed is required. Meanwhile, as either lateral forces or lateral slips of wheels were ignored, the algorithms proposed are not applicable where the accurate path following at relatively high speed is desired.

Satisfying the non-holonomic constraint in the path tracking of off-road vehicles is very challenging due to the existence of longitudinal and lateral slips at the four independent wheels. Some methods were proposed to restrict steering angles within small ranges for minimizing the slips at the wheels [Langson and Alleyne, 1997] [Yavin, 2003]. However, this leads to limited maneuverability of the vehicle due to the restricted steering angles. In the case of kinematic models, for a chosen instantaneous centre of rotation (ICR), the steering angles of all four wheels can be geometrically determined. However, in a slip situation, maintaining this ICR becomes impossible and the desired steering angles obtained through Ackermann formula becomes unusable [Selekwa and Nistler, 2011]. An attempt to locate the ICR using the yaw rate is presented in [Connette *et al.*, 2009]. The complexity of the controller development is evident in many works available in the literature. In this

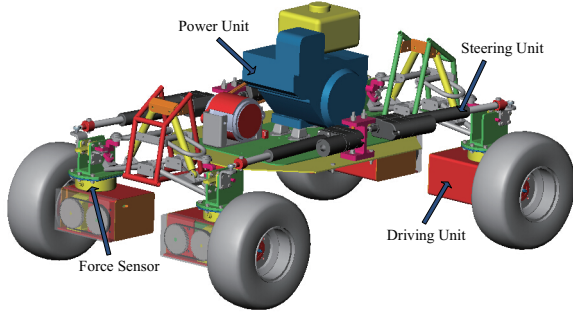


Figure 1: Mechanical System of 4WD4WS vehicle

work, the slip angles at the wheels are considered in the building of the vehicle dynamic model and used for the determination of the ICR.

As shown in Fig. 1, the platform used in this work is a four-wheel drive and four-wheel steering (4WD4WS) vehicle. The driving unit composed by a DC motor and a gear box provides the drive forces needed at each wheel. Four six-dimensional force sensors are installed on the driving units to detect the residual drive forces and lateral forces acting on the four independently controlled wheels. The aim of this work is to plan the path, calculate the desired forces and steering angles at each of the wheels and then control the steering and propulsion to guide the vehicle in tracking the planned path. To the best of authors' knowledge, the work presented in this paper is the first attempt to use independent force and steering control at individual wheel unit subsystems to guide a 4WD4WS vehicle.

The paper is organized as follows: Section 2 presents a path planning method by 7-order Bézier curves. Section 3 describes the dynamic model of 4WD4WS robot applied for force control. The design of P-controller and PI-controller for independent wheels is presented in Section 4. Conclusions are given in Section 5. The Appendix I gives detailed math for the determination of 7-order Bézier curves, and Appendix II provides some mathematical relationships used in the dynamic model.

2 Path Planning

The forces for controlling the vehicle are to be obtained using the desired path and the associated kinematic parameters along the path. In this work, Bézier curves are used to obtain such path and the desired forces.

2.1 Bézier Curves

Bézier curve was devised by Pierre Bézier in 1962 for the design of car bodies in the automobile industry [Joan-Arinyo, 1998]. Different from other kinds of 2D curves, Bézier curves only pass through the start and final control points, and the intermediate control points define the start and the final orientation and the shape of the

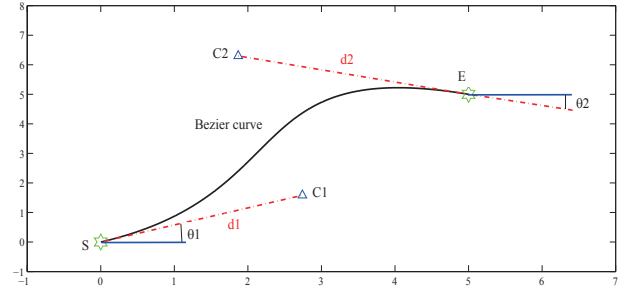


Figure 2: A cubic Bézier curve

curve as per [Zhou *et al.*, 2011]. Bézier curve always stay within the convex hull comprised by control points and is smoother than the cubic splines.

The parametric function of a Bézier curve is:

$$P(u) = \sum_{j=0}^n K_j^n(u) P_j, \quad 0 \leq u \leq 1 \quad (1)$$

where $K_j^n(u)$ is a Bernstein polynomial and P_j indicates the j^{th} control point.

Bézier curves are much more easier to define in contrast to some other kinds of curves. Given a start point $S(A_0, B_0)$ and an end point $E(A_3, B_3)$, by selecting the control points $C1(A_1, B_1)$ and $C2(A_2, B_2)$, a cubic Bézier curve can be obtained and is shown in Fig. 2.

The curvature $\kappa(u)$ at any point on the Bézier curve can be expressed in terms of the first and second derivatives of $x(u)$ and $y(u)$ with respect to u as in [Guechi *et al.*, 2009].

$$\kappa(u) = \frac{1}{R(u)} = \frac{x'(u)y''(u) - y'(u)x''(u)}{[x'(u)^2 + y'(u)^2]^{3/2}} \quad (2)$$

2.2 Order Determination for Bézier Curve

Due to outstanding properties of Bézier curves, many studies have been carried out in applying Bézier curves in the path planning of ground robots. K. G. Jolly used 3-order Bézier curve in Robot Soccer System [Jolly *et al.*, 2009]. The cubic Bézier curves were also applied in the path planning of AGV and mobile robots [Petrinec and Kovacic, 2005] [Niu *et al.*, 2008]. One significant limitation of the above studies is that only a single Bézier curve was generated to guide the robot at cornering. These methods will not be applicable when it comes to long path planning, which is normally composed by many successive straight lines and corners.

One important constraint in path planning is that the curvature along the path needs to be continuous. Ji-Wung developed path planning algorithm by 5-order Bézier curves [Jung Choi *et al.*, 2010]. Based on the curvature formula in (2), for two adjacent Bézier curves $P(u)$ and $Q(u)$ shown in Fig. 3, if the first and second

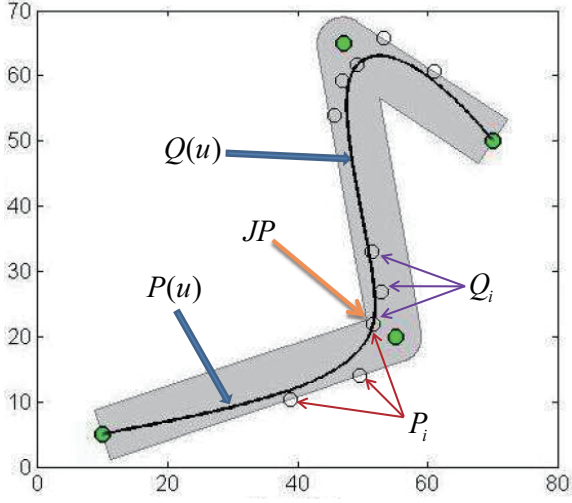


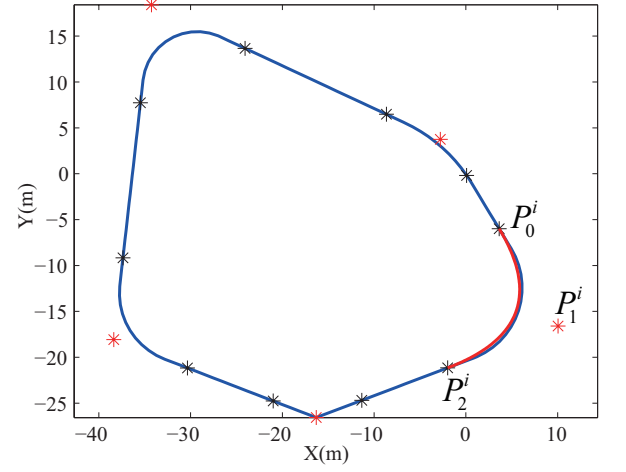
Figure 3: Path planning by 5-order Bézier curve

derivatives of $P(u)$ and $Q(u)$ are equal at the junction node JP , the curvature at JP is continuous. According to the conclusion stated in [wung Choi *et al.*, 2010], for curvature continuity, the minimum order of all Bézier curve segments is 5, or the curvature at start point of any Bézier curve will not only be determined by the control points near the start point but also by those near the end point of the curve. In other words, at least 6 control points need to be defined for each segment.

As the curvature reflects the change rate of tangential angles along the path, the path defined by 5-order Bézier curves can realize the continuity of yaw rate which is essential for ground vehicles controlled by wheel velocity at kinematic level. However, in this work, force control will be applied on wheels to guide a 4WD4WS vehicle, and the angular acceleration along the path needs to be continuous accordingly. It means that, for applying Bézier curves in path planning, the order of Bézier curve segments needs to be at least increased to 7, and 8 control points should be specified for each segment.

2.3 Path Planning by Bézier Curve

In this work, one of the aims is to generate a number of successive Bézier curve segments. These segments are linked end-to-end to compose the desired path that has continuity in position, tangent angle and curvature for the vehicle to track while its wheels are under force control. After determining the order of the Bézier curves, there are still two issues that need to be addressed. The first issue is that, as shown in (1), the Bézier curve is parameterized by u , which should be replaced by t in time domain for the vehicle to track the predefined path. The second one is that, as discussed above, 8 control points need to be specified for each segment.


 Figure 4: Estimation of Bézier curve segment length S_i

Replacing u by t

To replace variable u by t in time domain, G. Yang *et al* defined u as the ratio between the integration of tangent velocity V_t and the length of the curved path. As V_t is defined in time domain, u can be transferred to $u(t)$ which is a function of travel time t . The expression of $u(t)$ is presented in (3) [Yang and Choi, 2013].

$$u(t) = \frac{\int_0^t V_t(t) dt}{S_B} \quad (3)$$

where the curve length S_B can be calculated by the control points predefined. If the vehicle was supposed to complete the path with constant velocity v_0 , the travel time t can be obtained by S_B/v_0 . As the constant velocity v_0 has been used instead of the inherent velocity of Bézier curve characterized by the first derivative of (1), there were original errors existed between the predefined path and the tracking path under velocity profile v_0 before the implementation of control.

In this study, the main idea of introducing t into Bézier curve is to replace u by t/T^i , where T^i is the time for completing the current Bézier curve segment with desired average tangent velocity V_a which is specified as $3m/s$ in this work, and t varies from 0 to T^i . Hence, the problem becomes how to estimate segment length S^i .

Fig. 4 shows an original path, in which the curvature is not continuous at junction points between straight lines and arcs. There is also sharp corner exists, which is difficult for the vehicle to track. This study will use 7-order Bézier curve segments to track the original path and achieve curvature continuity. To estimate the curve length S^i , 2-order Bézier curve is applied. As shown in Fig. 4, for corner i , the start point P_0^i and the end point P_2^i can be selected on straight lines around junction points, and P_1^i is the intersection of two adjacent straight

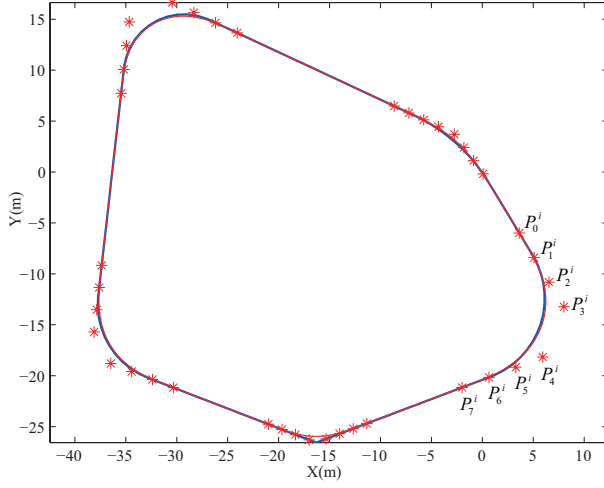


Figure 5: Planned path with Bézier curve segments

lines. By these three control points, a 2-order Bézier curve can be generated by (4) and shown as red curve in Fig. 4. T^i can be calculated by (5).

$$P^i(u) = (1-u)^2 P_0^i + 2(1-u)u P_1^i + u^2 P_2^i \quad (4)$$

$$T^i = \frac{S^i}{V_a} = \frac{\int_0^1 \sqrt{\dot{P}_x^i(u)^2 + \dot{P}_y^i(u)^2} du}{V_a} \quad (5)$$

As discussed above, for the path planning used for dynamic model, 7-order Bézier curve segments need to be built to realize the continuity of angular acceleration. After obtaining T^i , the 7-order Bézier curve function with variable t can be expressed by (6).

$$P^i(t) = \sum_{j=0}^7 K_j^7\left(\frac{t}{T^i}\right) P_j^i, \quad 0 \leq t \leq T^i \quad (6)$$

To determine the equation in (6), 8 control points from P_0^i to P_7^i need to be specified for each segment.

Choosing 8 control points

For segment i , the start control point P_0^i and the end control point P_7^i can be located by the start point and desired end point within the segment. The equations for P_0^i and P_7^i are presented in (7).

$$\begin{cases} P_0^i = P_{start}^i \\ P_7^i = P_{end}^i \end{cases} \rightarrow P_0^i, P_7^i \quad (7)$$

The control point P_1^i can be calculated by solving the equations composed by longitudinal and lateral velocities. In this work, for every start point within segment, the longitudinal velocity (V_{ls}) is V_a and lateral velocity

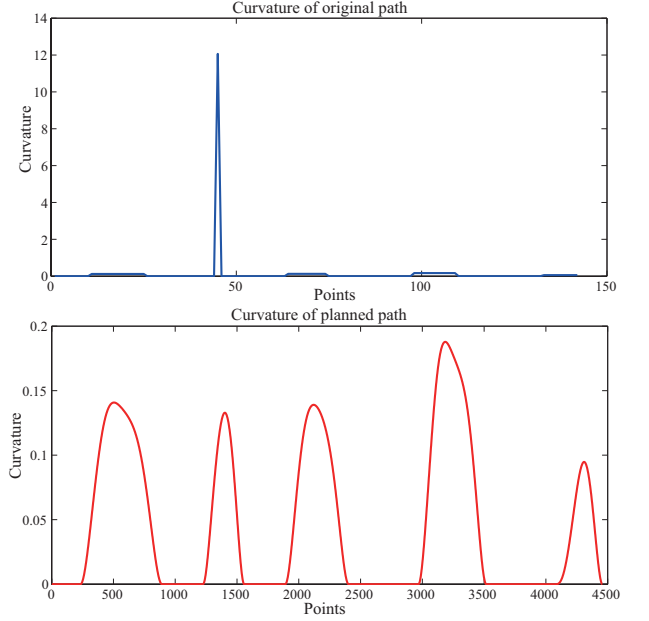


Figure 6: Curvature of original path and planned path

(V_{Ls}) should always be 0. P_1^i can be obtained by (8).

$$\begin{cases} V_{ls} = V_a \\ V_{Ls} = 0 \end{cases} \rightarrow P_1^i \quad (8)$$

By using the second and third derivatives of 7-order Bézier curve equation and making $t = 0$, the expressions for longitudinal acceleration (a_s) and curvature (C_s) at the start point can be obtained. Solving these two equations by defining a_s and C_s equal to 0, the control point P_2^i can be obtained by (9).

$$\begin{cases} a_s = 0 \\ C_s = 0 \end{cases} \rightarrow P_2^i \quad (9)$$

In the same way, the expressions for angular acceleration (α_s) and change rate of longitudinal acceleration (J_s) can also be deduced, and P_3^i can be calculated by solving (10).

$$\begin{cases} \alpha_s = 0 \\ J_s = 0 \end{cases} \rightarrow P_3^i \quad (10)$$

The detailed expressions for (8), (9) and (10) are given in the Appendix I.

The last 4 control points can be calculated in the same manner as above, and the sequence for getting P_4^i to P_7^i is listed in (11).

$$P_7 \rightarrow P_6 \rightarrow P_5 \rightarrow P_4 \quad (11)$$

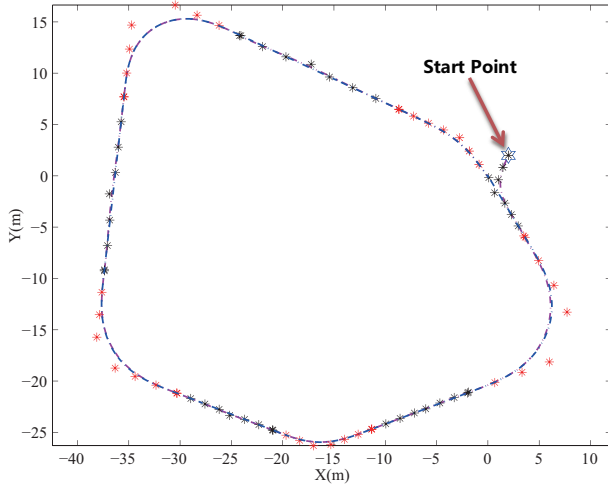


Figure 7: Tracking planned path

After computing all 8 control points for Bézier curve segments in the corners of original path, the planned path can be generated and shown in Fig. 5, in which the planned path is very close to the original path. Fig. 6 shows the curvature distribution along the original path and planned path. Obviously, the curvature becomes continuous after path planning.

To track the planned path shown in Fig. 5, the above path planning algorithm can be applied regardless of where the start point of vehicle locates. Fig. 7 shows the predefined tracking path of vehicle, in which the straight lines on planned path are tracked by 7-order Bézier curves as well.

As all Bézier curve segments have been obtained, the profiles for vehicle velocity, longitudinal and lateral acceleration, yaw rate and angular acceleration can be generated along the whole tracking path. These parameters are all continuous and shown in Fig. 8. As these reference parameters are for the mass center, to figure out the steering angles and drive forces for the control of the vehicle, the dynamic model of 4WD4WS vehicle needs to be built.

3 Dynamic Model of 4WD4WS Vehicle

The model used in this study is a 4WD4WS vehicle, which is equipped with four independent force sensors on four driving/steering modules for detecting drive forces and lateral forces acting on the wheels.

Drive forces and lateral forces acting on wheels are the two main external forces that govern the dynamics of ground vehicles, and contribute to the majority of the efforts for path tracking of vehicles. This work will focus on these two types of forces at each wheel to guide the vehicle along the planned path.

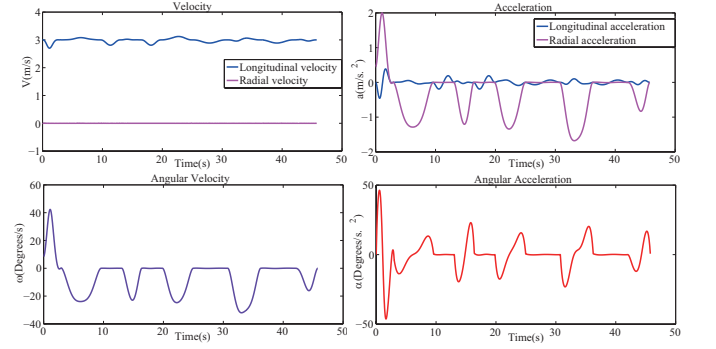


Figure 8: Profiles of kinematic parameters

3.1 Lateral Forces

When a vehicle is cornering, tires generate appropriate lateral forces to guide the vehicle along a certain path. The lateral forces cause the tyres to deform and as a result, the actual travelling direction of the tire differs from the wheel centre plane by the slip angle [Koo *et al.*, 2004].

The relationship between lateral forces and slip angles is illustrated by tire lateral characteristic curve in [Baffet *et al.*, 2006]. From this characteristic curve, when slip angle is under 5 degrees, the lateral force F_L has a linear relationship with slip angle α :

$$F_L = C_L \alpha, \quad -5^\circ \leq \alpha \leq 5^\circ \quad (12)$$

The cornering stiffness C_L varies considerably depending on the vertical loads on the vehicle and different types of tires. Note that positive α causes negative F_L .

3.2 Dynamic Model of 4WD4WS Vehicle

The forces acting on the 4WD4WS vehicle are illustrated in Fig. 9. As the vehicle is considered as a rigid body, the ICR is determined by wheel velocities as well as the slip velocities. All resultant velocities are perpendicular to the lines joining those points to the ICR.

For wheel i , the relationship among steering angle δ_i , slip angle α_i and sideslip angle β_i is expressed as:

$$\delta_i = \beta_i - \alpha_i, \quad i = 1, \dots, 4 \quad (13)$$

In (13), when wheel i turn left, δ_i and β_i are defined as positive values, and α_i is defined as a negative value. Inversely, if wheel i was in right posture, δ_i and β_i are negative, and α_i is positive.

To let the vehicle travel along the desired path, the longitudinal velocity at centre of gravity (CG) should always be tangent to the path. In other words, the velocity at CG is perpendicular to the line between ICR and CG. Based on geometric relationships shown in Fig. 9,

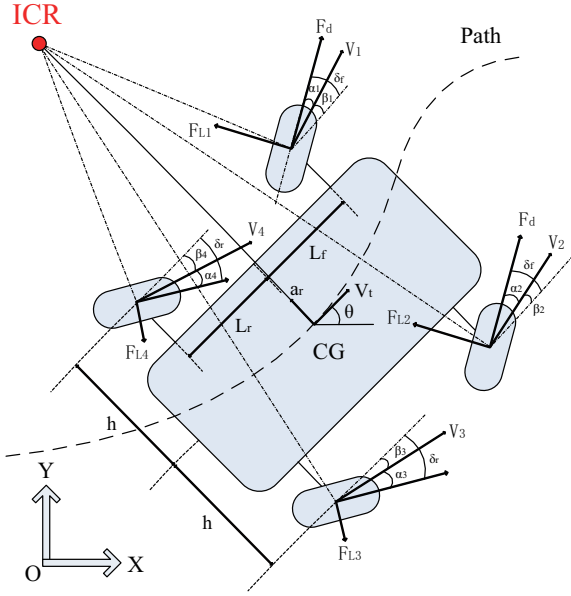


Figure 9: Dynamic model of 4WD4WS vehicle

the reference values of β_i can be obtained as:

$$\begin{cases} \beta_1(t) = \tan^{-1} \left(\frac{\dot{\theta}(t)L_f}{V_t(t) - \dot{\theta}(t)h} \right) \\ \beta_2(t) = \tan^{-1} \left(\frac{\dot{\theta}(t)L_f}{V_t(t) + \dot{\theta}(t)h} \right) \\ \beta_3(t) = -\tan^{-1} \left(\frac{\dot{\theta}(t)L_r}{V_t(t) + \dot{\theta}(t)h} \right) \\ \beta_4(t) = -\tan^{-1} \left(\frac{\dot{\theta}(t)L_r}{V_t(t) - \dot{\theta}(t)h} \right) \end{cases} \quad (14)$$

where $\dot{\theta}(t)$ and $V_t(t)$ can be obtained by path planning algorithm presented in Section 2.

By dynamic analysis, for tracking the desired path, the vehicle should meet the requirements of longitudinal acceleration a_t , radial acceleration a_r and angular acceleration $\ddot{\theta}$. In this work, the system inputs are F_d, δ_f and δ_r . F_d is the algebraic sum of rolling resistance and drive force acting on each of front wheels, and is called the residual drive force. The steering angles of front wheels are considered to be equal and denoted by δ_f . δ_r is the steering angle of the rear wheels. The residual drive forces of rear wheels will be kept zero in this work.

The dynamic equations for 4WD4WS vehicle are listed as follows:

$$\begin{cases} 2F_d \cos \delta_f - \sum F_{L12} \sin \delta_f - \sum F_{L34} \sin \delta_r \\ = ma_t \\ 2F_d \sin \delta_f + \sum F_{L12} \cos \delta_f + \sum F_{L34} \cos \delta_r \\ = mV_t^2 \text{sign}(\kappa)/R \\ 2F_d \sin \delta_f L_f + \sum F_{L12} \cos \delta_f L_f - \sum F_{L34} \\ \cos \delta_r L_r + \Delta F_{L12} \sin \delta_f h - \Delta F_{L34} \sin \delta_r h \\ = I\ddot{\theta} \end{cases} \quad (15)$$

Parameter	Value	Units	Description
m	100	kg.	Vehicle weight
m_d	10	kg.	Driving unit weight
I	4	kg.m ²	Inertia
a_{rmax}	6	m/s ²	Max. radial acceleration
L_r	0.6	m.	Length: CG to rear
L_f	0.8	m.	Length: CG to front
h	0.3	m.	Half width

where $\sum F_{L12} = (F_{L1} + F_{L2})$, $\sum F_{L34} = (F_{L3} + F_{L4})$, $\Delta F_{L12} = (F_{L1} - F_{L2})$ and $\Delta F_{L34} = (F_{L3} - F_{L4})$.

According to (13) and the constrains that $\delta_1 = \delta_2 = \delta_f$ and $\delta_3 = \delta_4 = \delta_r$, the relationship between slip angles can be expressed by:

$$\begin{cases} \alpha_2 = \alpha_1 - \beta_1 + \beta_2 \\ \alpha_3 = \alpha_4 + \beta_3 - \beta_4 \end{cases} \quad (16)$$

To apply the linear relationship between lateral force and slip angle, it is assumed that all slip angles are small and specified as $|\alpha_i| \leq 5^\circ$, $i = 1, \dots, 4$. The expression for lateral force in (12) can be substituted into (15). Considering (16) and removing F_d using (15), the relationship between α_1 and α_4 can be expressed as:

$$C_L \Delta \beta_{12} \sin(\beta_1 - \alpha_1)h - C_L(2\alpha_4 + \Delta \beta_{34}) \cos(\beta_4 - \alpha_4) \\ (L_f + L_r) - C_L \Delta \beta_{34} \sin(\beta_4 - \alpha_4)h = I\ddot{\theta} - ma_r L_f \quad (17)$$

where $\Delta \beta_{12} = (\beta_1 - \beta_2)$, $\Delta \beta_{34} = (\beta_3 - \beta_4)$ and $a_r = V_t^2 \text{sign}(\kappa)/R$.

For small angles, α_1 can be expressed by α_4 as:

$$\alpha_1 = C\alpha_4^2 + D\alpha_4 + E \quad (18)$$

where coefficients C, D, E are given in the Appendix II.

Using the first two equations of (15), another relationship between α_1 and α_4 can be obtained as follows,

$$2C_L \alpha_1 - C_L \Delta \beta_{12} + C_L(2\alpha_4 + \Delta \beta_{34}) \\ [\cos \Delta \beta_{14} - (\alpha_4 - \alpha_1) \sin \Delta \beta_{14}] \\ = ma_r (\cos \beta_1 + \alpha_1 \sin \beta_1) \\ - ma_t (\sin \beta_1 - \alpha_1 \cos \beta_1) \quad (19)$$

where $\Delta \beta_{14} = (\beta_1 - \beta_4)$.

Considering small angles and substituting (18) into (19),

$$F\alpha_4^3 + G\alpha_4^2 + H\alpha_4 + K = 0 \quad (20)$$

where F, G, H and K are coefficients which contain constant parameters of the system and the kinematic parameters obtained from path generation. Expressions of F, G, H and K are listed in the Appendix II.

The value of α_4 can be obtained as the smallest real root of all potential solutions to (20). Then, α_1 can be

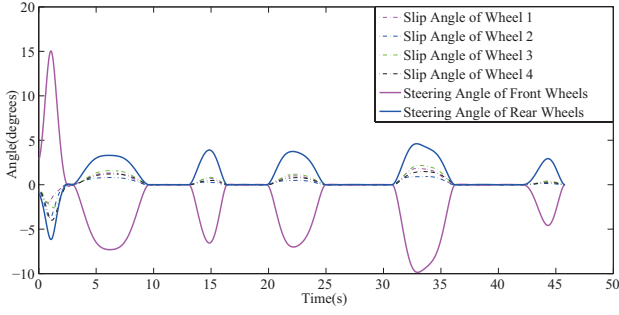


Figure 10: Reference steering angles and slip angles

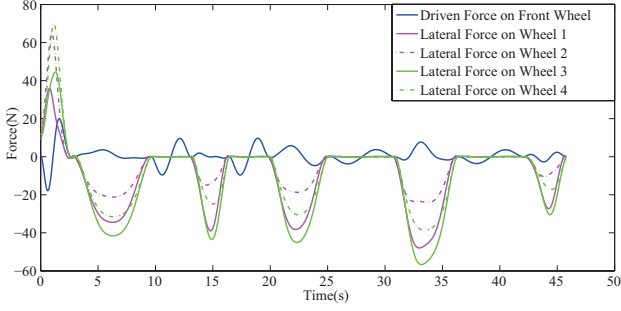


Figure 11: Reference driven forces and lateral forces

obtained from (18), α_2 and α_3 can be obtained from (16), steering angles δ_f and δ_r can be calculated from (13), and the residual drive force of front wheels F_d can be obtained using the first equation of (15).

To verify the feasibility of dynamic model built, simulations were carried out. Based on the constant parameters of 4WD4WS vehicle listed in Table 1, input the profiles shown in Fig. 8 into the dynamic model in (15), the reference values of steering angles and drive forces on four wheels can be calculated and shown in Fig. 10 and Fig. 11 respectively. In this work, the planned path is composed by 10 successive Bézier curve segments, in which 10 corresponding cornering stiffness C_L vary from -1000 to -4200 were selected in the simulation. In the future work, C_L will be obtained by measuring the lateral forces and slip angles on tires of vehicle and inputted into control system in real-time. In Fig. 10, it can be seen that all slip angles locate within the range from -5 degrees to +5 degrees. Hence, the assumption that slip angles are small is valid.

3.3 Force Sensor Model

In this work, the control of drive forces on wheels is based on the forces sensed by force sensors. Hence, the force profile acting on force sensors needs to be calculated in advance. Fig. 12 shows the forces acting on one driving unit of the vehicle, in which the force sensed by force sensor can be obtained by (21).

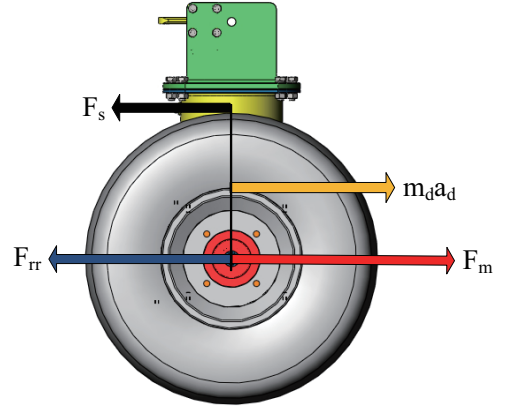


Figure 12: Force sensor model of 4WD4WS vehicle

$$F_s = F_d - m_d a_d \quad (21)$$

Where F_d is the residual drive force in (15), m_d and a_d are the mass and acceleration of driving unit. As drive force control will be applied on the outputs of drive motors, the reference data for drive forces of motors needs to be calculated. The motor drive force F_m is expressed in (22)

$$F_m = F_d + F_{rr} \quad (22)$$

Where F_{rr} is the rolling resistance on wheel which can be calculated by equation in (23).

$$\begin{cases} F_{rr} = K_{rr} V_w & 0 \leq V_w \leq 5 \\ F_{rr} = f_{cons} & 5 < V_w \end{cases} \quad (23)$$

Where V_w is the wheel speed, K_{rr} is the linear coefficient that is specified as 0.008 in the simulation, and constant f_{cons} is 0.04. Force sensor is normally modeled as a spring with Stiffness K_s and damping coefficient C_s . In this study, the equation for force sensor model is presented in (24).

$$F_s = K_s x + C_s \dot{x} \quad (24)$$

Based on the force sensor model built in this section, the profile of forces acting on force sensors can be generated. Fig. 13 shows the F_s sensed by force sensors on driving units. Note that F_s was calculated based on the condition that the residual drive force is F_s for front wheels, and is 0 for the rear wheels.

4 Controllers Design for 4WD4WS Vehicle

To guide the 4WD4WS vehicle to track the predefined path by maintaining the profiles of kinematic parameters generated, the controllers for steering angles and drive forces on wheels need to be designed. In this work,

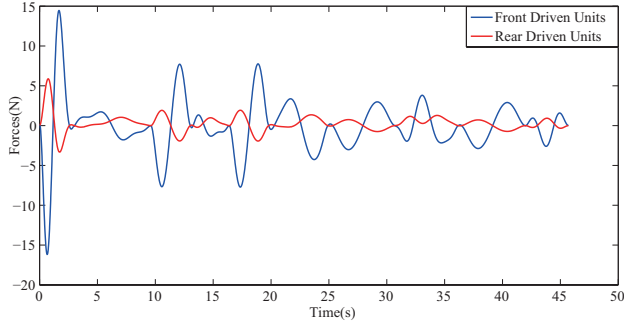


Figure 13: Force profiles on force sensors

the control parameters include δ_f (front steering angle) and δ_r (rear steering angle) shown in Fig. 10, and F_{sf} (force sensed by front sensors) and F_{sr} (force sensed by rear sensors) shown in Fig. 13. The forces felt by all four wheels may also differ, yet, as the force control is individually carried out at each wheel, this does not pose a problem.

4.1 P-Controller for Drive Forces

The output torque of DC motor is directly proportional to the electrical current in the rotor armature [Dimitry M. Gorinevsky *et al.*, 1997]. The equation for output torque can be expressed in (25).

$$M_G = \frac{M_s}{U_c} E_{ff} u \quad (25)$$

where M_s is the starting torque, U_c is the nominal voltage, u is the voltage supplied, and M_s/U_c is specified as 3.275 according to motor parameters. E_{ff} is the efficiency of motor which is evaluated as 0.86. M_G is the output torque which can be expressed by motor drive force F_m and wheel radius R_w in (26).

$$M_G = F_m R_w \quad (26)$$

Considering the proportional relationship between motor torque and current supplied, P-control was applied in controller design and shown in (27)

$$\Delta u(k) = K_{Pf}(e_f(k) - e_f(k-1)) \quad (27)$$

where K_{Pf} is the gain of P-controller and is designed as 0.03. $e_f(k)$ denotes the error between force sensed and reference value.

4.2 PI-Controller for Steering Angles

The steering unit is modeled as a DC motor together with a gearbox which is used to achieve the steering motions of driving unit by the position control of motor. The position control can be realized by regulating the speed of motor based on the position error emerged. As

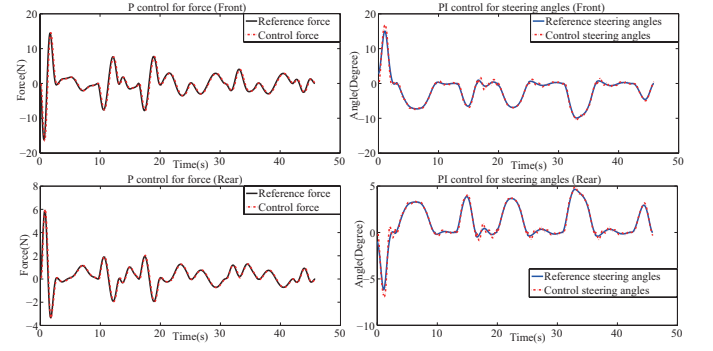


Figure 14: Results of P control and PI control

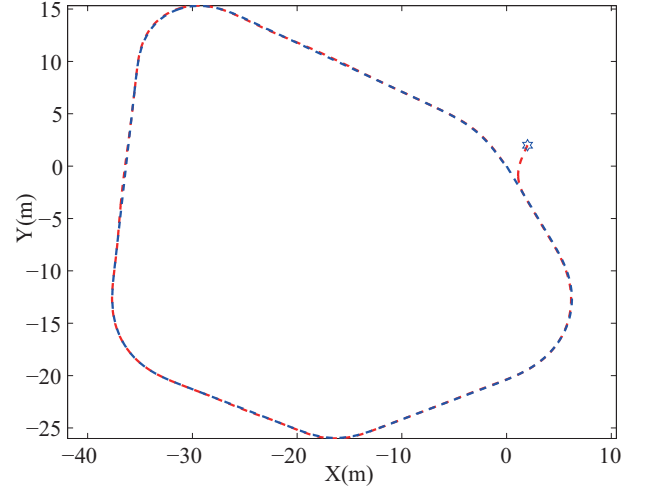


Figure 15: Actual tracking path under control

the output speed of DC motor has non-linear relationship with voltage, this work applied PI-control, in which I-control can be used to eliminate the steady-state deviation accumulated.

According to parameters of motor and gearbox, the system transfer function of steering unit used in this study can be obtained and presented in (28).

$$G_p(s) = \frac{\omega(s)}{U(s)} = \frac{1.785}{0.0021s^2 + 0.17s + 1} \quad (28)$$

After discretization, the rotary speed of motor can be expressed by:

$$\omega(k) = 1.4302\omega(k-1) - 0.4618\omega(k-2) + 0.0318u(k-1) + 0.0246u(k-2) \quad (29)$$

Given sample time p , the steering angle can be calculated by:

$$\delta(k) = \delta(k-1) + \omega(k-1)p \quad (30)$$

For PI-control, the controller for steering motion can be designed as:

$$\Delta u(k) = K_{Ps}(e_\delta(k) - e_\delta(k-1)) + K_{Is}e_\delta(k) \quad (31)$$

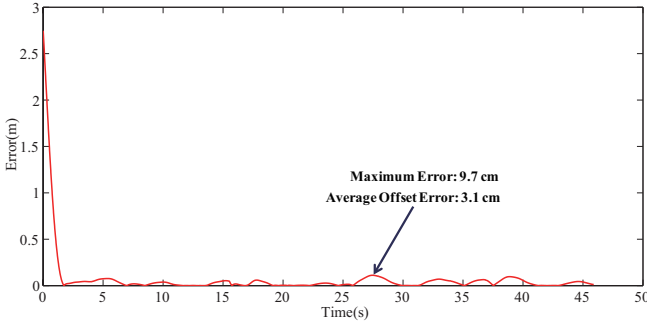


Figure 16: Offset error along the path

Where K_{Ps} and K_{Is} are designed as 3.42 and 0.1408 respectively in this work.

4.3 Simulation Results for Control

As illustrated in Section 2, the planned path is composed of 10 successive 7-order Bézier curve segments. In the application of controllers designed, the initial kinematic conditions (velocities, accelerations, angular accelerations, etc) are generated by the efforts of control applied in the completion of last Bézier curve segment, and will be used for the generation of next segment, from which the force and steering profiles can be obtained for the control in next segment tracking.

Fig. 14 shows the results of maintaining profiles by controllers designed. The actual tracking path under control is shown in Fig. 15, in which the tracking path is very close to the planned path. As indicated in Fig. 16, after getting back to the reference path, the maximum offset error along the path is within 10 cm and the average offset error is 3.1 cm.

5 Conclusion

The paper has presented a method that plan the path with curvature continuity by 7-order Bézier curve segments. In the same way, the tracking segments can be generated to provide the profiles of kinematic parameters. Considering the lateral forces acting on wheels, the dynamic model used for independent force control was built, and the reference drive forces and steering angles for each segment can be calculated by inputting the obtained kinematic profiles into this model. Finally, P-controller and PI-controller were designed for the drive forces and steering angles of four independent wheels. The relevant simulation results show that force and position controllers can be implemented at each of the wheels independently and the accurate navigation of the vehicle can be achieved. In future work, methods will be developed to estimate the slip stiffness in real-time, and experiments will be carried out on the 4WD4WS vehicle developed at authors' laboratories to verify the validity of methods proposed in this work.

Appendix I

$$V_{ls} = 7\left(\frac{1}{T^i}\right)(K_{1x} \cos(\theta_0) + K_{1y} \sin(\theta_0))$$

$$V_{Ls} = 7\left(\frac{1}{T^i}\right)(K_{1x} \sin(\theta_0) - K_{1y} \cos(\theta_0))$$

$$a_s = 42\left(\frac{1}{T^i}\right)^2(K_{2x} \cos(\theta_0) + K_{2y} \sin(\theta_0))$$

$$C_s = 294\left(\frac{1}{T^i}\right)^3(K_{1x}K_{2y} - K_{1y}K_{2x})/W_{xy}^{\frac{3}{2}}$$

$$J_s = 210\left(\frac{1}{T^i}\right)^3(K_{3x} \cos(\theta_0) + K_{3y} \sin(\theta_0))$$

$$\alpha_s = 1470\left(\frac{1}{T^i}\right)^4(K_{1x}K_{3y} - K_{1y}K_{3x})/W_{xy} - 172872\left(\frac{1}{T^i}\right)^6$$

$$(K_{1x}K_{2y} - K_{1y}K_{2x})(K_{1x}K_{2x} + K_{1y}K_{2y})/W_{xy}^2$$

Where,

$$K_{1x} = P_{1x}^i - P_{0x}^i$$

$$K_{1y} = P_{1y}^i - P_{0y}^i$$

$$K_{2x} = P_{2x}^i - 2P_{1x}^i + P_{0x}^i$$

$$K_{2y} = P_{2y}^i - 2P_{1y}^i + P_{0y}^i$$

$$K_{3x} = P_{3x}^i - 3P_{2x}^i + 3P_{1x}^i - P_{0x}^i$$

$$K_{3y} = P_{3y}^i - 3P_{2y}^i + 3P_{1y}^i - P_{0y}^i$$

$$W_{xy} = 49\left(\frac{1}{T^i}\right)^2((P_{1x}^i - P_{0x}^i)^2 + (P_{1y}^i - P_{0y}^i)^2)$$

Note that θ_0 indicates the orientation at start point.

Appendix II

$$A = I\ddot{\theta}_d - \frac{mV_t^2}{R} \text{sign}(\kappa)L_f$$

$$B = C_L(\beta_1 - \beta_2) \cos \beta_1 h$$

$$C = -2C_L(L_f + L_r) \sin \beta_4/B$$

$$D = (-2C_L(L_f + L_r) \cos \beta_4 + C_L h(\beta_3 - \beta_4) \cos \beta_4)/B$$

$$- C_L(L_f + L_r)(\beta_3 - \beta_4) \sin \beta_4$$

$$E = (C_L h(\beta_1 - \beta_2) \sin \beta_1 - C_L h(\beta_3 - \beta_4) \sin \beta_4$$

$$- C_L(L_f + L_r)(\beta_3 - \beta_4) \cos \beta_4 - A)/B$$

$$F = 2C_L \sin(\beta_1 - \beta_4)C$$

$$G = 2C_L C - C_L \sin(\beta_1 - \beta_4)(2 - 2D - (\beta_3 - \beta_4)C)$$

$$- ma_r C \sin \beta_1 - ma_t C \cos \beta_1$$

$$H = 2C_L D + 2C_L \cos(\beta_1 - \beta_4)$$

$$- C_L \sin(\beta_1 - \beta_4)(\beta_3 - \beta_4 - 2E - \beta_3 D + \beta_4 D)$$

$$- ma_r \sin \beta_1 D - ma_t D \cos \beta_1$$

$$K = 2C_L E - C_L(\beta_1 - \beta_2) + C_L \cos(\beta_1 - \beta_4)(\beta_3 - \beta_4)$$

$$+ C_L \sin(\beta_1 - \beta_4)(\beta_3 - \beta_4)E - ma_r \cos \beta_1$$

$$- ma_r E \sin \beta_1 + ma_t \sin \beta_1 - ma_t E \cos \beta_1$$

Note that $\ddot{\theta}_d$ is the desired acceleration from path generation.

References

- [Baffet *et al.*, 2006] G. Baffet, A. Charara, and J. Stephant. Sideslip angle, lateral tire force and road friction estimation in simulations and experiments. *Proceedings of the IEEE International Conference on Control Applications*, pages 903–908, 2006.
- [Connette *et al.*, 2009] C.P. Connette, C. Parltitz, M. Hagele, and A. Verl. Singularity avoidance for over-actuated, pseudo-omnidirectional, wheeled mobile robots. *IEEE International Conference on Robotics and Automation*, pages 4124–4130, 2009.
- [Dimitry M. Gorinevsky *et al.*, 1997] A.M.F.A.Y.U.S. Dimitry M. Gorinevsky, A.M. Formalsky, and A.Y.U. Schneider. Force control of robotics systems. *CRC Press LLC*, 1997.
- [Guechi *et al.*, 2009] E. Guechi, J. Lauber, M. Dambrine, S. Blazic, and G. Klancar. Tracking-error model-based pdc control for mobile robots with acceleration limits. *Fuzzy Systems-IEEE*, pages 197–202, 2009.
- [Iagnemma and Dubowsky, 2004] Karl Iagnemma and Steven Dubowsky. Traction control of wheeled robotic vehicles in rough terrain with application to planetary rovers. *The International Journal of Robotics Research*, 23(10-11):1029–1040, 2004.
- [Joan-Arinyo, 1998] Robert Joan-Arinyo. Geometric modeling. second edition. *Computer-Aided Design*, 30(8), 1998.
- [Jolly *et al.*, 2009] K.G. Jolly, R. Sreerama Kumar, and R. Vijayakumar. A bézier curve based path planning in a multi-agent robot soccer system without violating the acceleration limits. *Robotics and Autonomous Systems*, 57(1):23 – 33, 2009.
- [Koo *et al.*, 2004] S.-L. Koo, H.-S. Tan, and M. Tomizuka. Nonlinear tire lateral force versus slip angle curve identification. *Proceedings of the American Control Conference*, 3:2128–2133, 2004.
- [Langson and Alleyne, 1997] W. Langson and A. Alleyne. Multivariable bilinear vehicle control using steering and individual wheel torques. *American Control Conference*, 2:1136–1140, 1997.
- [Maalouf *et al.*, 2006] E. Maalouf, M. Saad, and H. Salih. A higher level path tracking controller for a four-wheel differentially steered mobile robot. *Robotics and Autonomous Systems*, 54(1):23–33, 2006.
- [Niu *et al.*, 2008] Guochen Niu, Lili Liu, Hao Chen, and Qingji Gao. Set-point stabilization of nonholonomic mobile robot based on optimizing bezier curve. *IEEE International Conference on Intelligent Control and Automation*, pages 1609–1612, 2008.
- [Petrinec and Kovacic, 2005] K. Petrinec and Z. Kovacic. The application of spline functions and bezier curves to agv path planning. *IEEE International Conference on Industrial Electronics*, 4:1453–1458, 2005.
- [Selekwa and Nistler, 2011] M.F. Selekwa and J.R. Nistler. Path tracking control of four wheel independently steered ground robotic vehicles. *Proceedings of the IEEE Conference on Decision and Control*, pages 6355–6360, 2011.
- [Tham *et al.*, 1999] Yew Keong Tham, Han Wang, and Eam Khwang Teoh. Multi-sensor fusion for steerable four-wheeled industrial vehicles. *Control Engineering Practice*, 7(10):1233–1248, 1999.
- [Waldron and Abdallah, 2007] K.J. Waldron and M.E. Abdallah. An optimal traction control scheme for off-road operation of robotic vehicles. *Mechatronics, IEEE/ASME Transactions on*, 12(2):126–133, 2007.
- [Wung Choi *et al.*, 2010] Ji wung Choi, Renwick E. Curry, and Gabriel Hugh Elkaim. Continuous curvature path generation based on bezier curves for autonomous vehicles. *International Journal of Applied Mathematics*, 40(2):91–101, 2010.
- [Yalcin *et al.*, 2006] M.K. Yalcin, S.M. Yesiloglu, M. Dal, and Hakan Temeltas. Maneuvering strategies for four-wheel drive, four-wheel steer mobile robots using curvatures based on weingarten-maps. *IEEE Industrial Electronics, IECON 2006*, pages 4148–4152, 2006.
- [Yang and Choi, 2013] G.J. Yang and B.W. Choi. Smooth trajectory planning along bezier curve for mobile robots with velocity constraints. *International Journal of Control and Automation*, 6(2):225–234, 2013.
- [Yavin, 2003] Y. Yavin. Modelling the motion of a car with four steerable wheels. *Mathematical and Computer Modelling*, 38(10):1029–1036, 2003.
- [Zhou *et al.*, 2011] F. Zhou, B. Song, and G. Tian. Bézier curve based smooth path planning for mobile robot. *Journal of Information and Computational Science*, 8(12):2441–2450, 2011.